Supplementary Information for

Electron-doping-induced destabilization of the dimerized insulating state in monolayer $IrTe_2$

Mingyung Lee,† Jae-Hyun Yun,†[b,c] Kyoo Kim,[d] Hyobeom Lee,[a] Woojin Choi,[a] Kyoungree Park,[a] Seha Lee,[a] Hayoon Im,[e] Choongyu Hwang,[e] Bo Gyu Jang,*[f] Sung-Kwan Mo,*[g] and Jinwoong Hwang*[a]

[a.] Department of Physics and Institute of Quantum Convergence Technology, Kangwon National University, Chuncheon 24341, Korea.

[b.] Department of Chemistry, Pohang University of Science and Technology, Pohang 37673, Korea.

[c.] Department of Applied Physics, Kyung Hee University, Yongin 17104, Korea.

[d.] Korea Atomic Energy Research Institute, Daejeon 34057, Korea.

[e.] Department of Physics, Pusan National University, Busan, Korea.

[f.] Department of Materials Science and Engineering, Kyung Hee University, Yongin 17104, Korea.

[g.] Advanced Light Source, Lawrence Berkeley National Laboratory, Berkeley, CA, USA.

†. equal contribution

*. Corresponding authors: bgjang@khu.ac.kr, SKMo@lbl.gov, jwhwang@kangwon.ac.kr

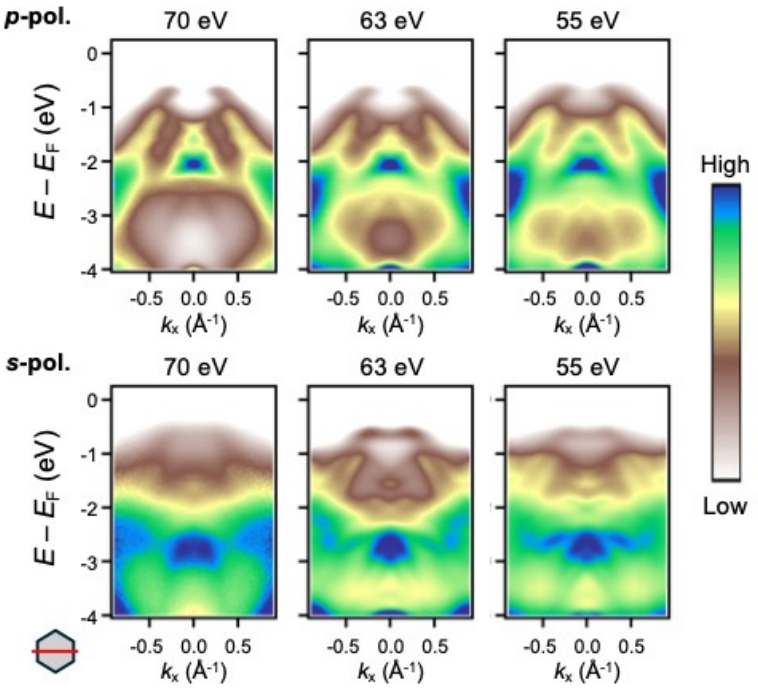

Figure S1. Photon energy dependent ARPES intensity maps of pristine ML $IrTe_2$ taken by 70 eV, 63 eV, and 55 eV using *p*-polarized (upper panels) and *s*-polarized photons (lower panels) at 20 K.

To clarify the origin of the apparent weak feature near the Fermi energy (E_F) observed in the momentum-second-derivative ARPES spectrum of pristine ML $IrTe_2$ (Fig. 3d), we systematically compared ARPES data acquired under multiple photon energies and polarizations.

As shown in Fig. **S**1, pristine ML $IrTe_2$ consistently exhibits an insulating electronic structure for all measured conditions, including *p*-polarized photons at 70, 63, and 55 eV, as well as *s*-polarized photons at the same energies. In all cases, the raw ARPES intensity maps show no band crossing or finite spectral weight reaching E_F, confirming the robust insulating nature of pristine ML $IrTe_2$. While the spectral intensity varies due to matrix-element effects, the absence of low-energy electronic states is independent of photon energy and polarization.

The momentum-second-derivative analysis (Fig. 3) was employed to enhance weak dispersive features near the band edges, particularly in the vicinity of E_F, where the signal is intrinsically weak. However, this method can also amplify small intensity gradients near the band edge, potentially generating artificial features. To verify the intrinsic electronic structure, we additionally performed energy-second-derivative analysis (Fig. **S**2), which more reliably preserves the gap structure. The absence of any dispersive feature approaching E_F in this analysis confirms that the apparent near-E_F feature in Fig. 3d originates from data processing rather than intrinsic electronic states

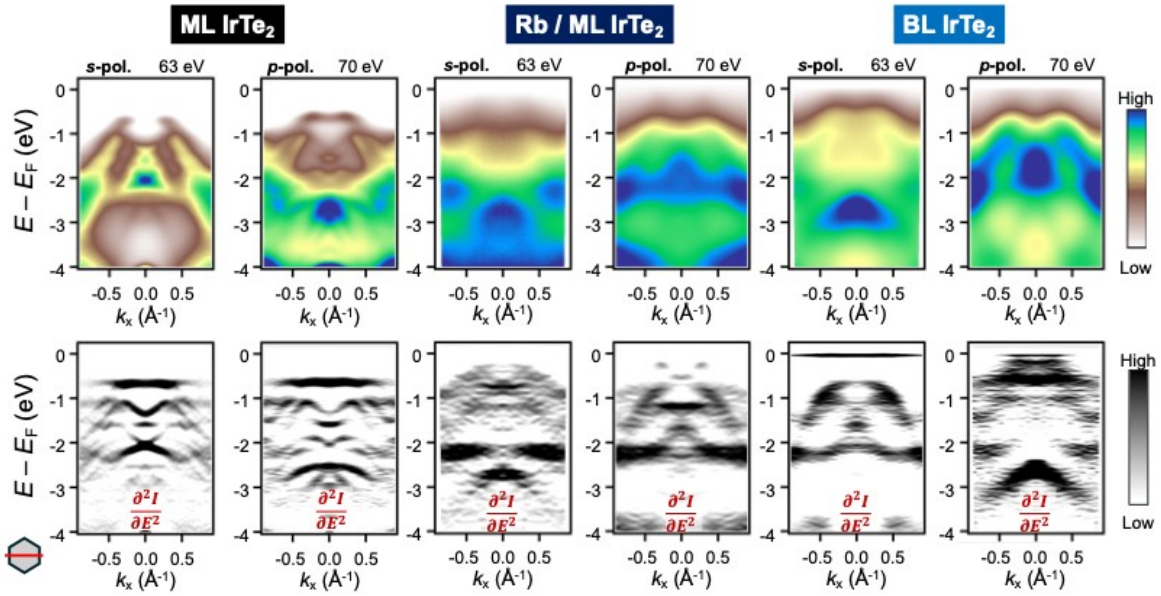

Figure S2. Raw (upper panel) and 2nd derivative ARPES intensity map with respect to energy (lower panel) for ML, Rb-dosed, and BL $IrTe_2$ films obtained by *p*-polarized 70 eV and *s*-polarized 63 eV photons at 20 K.

We performed additional orbital-resolved DFT calculations, as shown in Fig. **S**3, to further clarify the orbital character of the low-energy electronic states,

The results indicate that the states near the Fermi level do not originate from a single atomic orbital, but instead arise from strong hybridization between Ir 5*d* and Te 5*p* orbitals. Both contributions are significant, and the low-energy electronic structure is governed by these hybridized bands.

Upon electron doping, the Fermi level shifts upward into these hybridized states, indicating that the additional electrons occupy the Ir–Te hybridized bands. Within this framework, the change in Ir valence state observed in the core-level spectra reflects a modification of the Ir d-electron occupation within these hybridized states, while the Te 4d core-level shifts indicate the accompanying charge redistribution involving Te orbitals.

Therefore, the orbital-resolved analysis supports a picture in which electron doping modifies the occupation of the hybridized Ir–Te states, rather than filling a purely atomic-like Ir d band. This provides a consistent explanation for both the XPS results and the ARPES-observed band reconstruction.

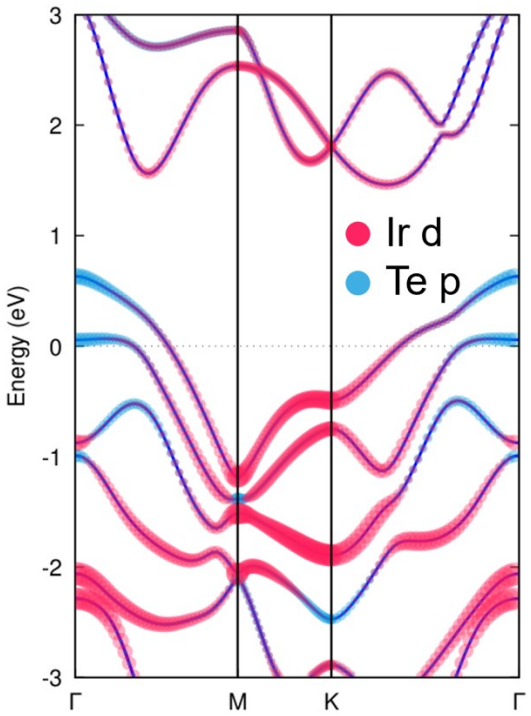

Figure S3. Orbital-resolved electronic band structure of ML $IrTe_2$. DFT band structure projected onto Ir *d* orbitals (ref) and Te *p* orbitals (blue). The color scale represents the orbital-resolved spectral weight, highlighting the relative contribution of each atomic orbital to the electronic states.

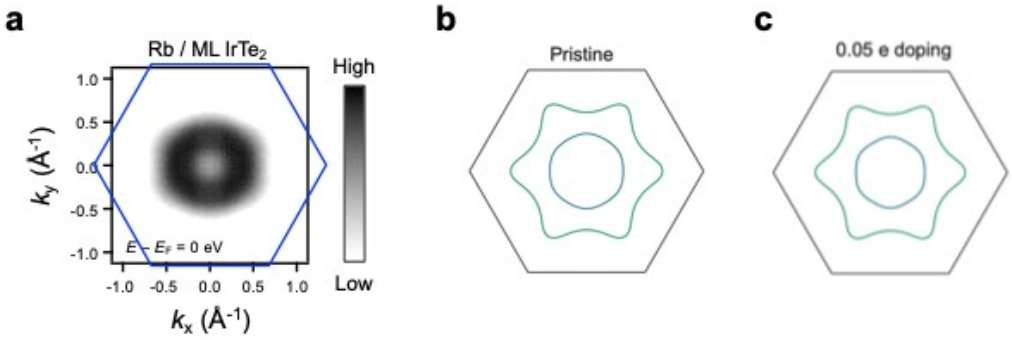

Figure S4. (a) ARPES Fermi surface map of Rb-dosed ML (Rb/ML) $IrTe_2$ taken by *p*-polarized 70 eV photons at 20 K. Blue hexagon presents the Brillouin zone of ML $IrTe_2$. (b,c) DFT-calculated Fermi surfaces of pristine (b) and 0.05 electron doped ML $IrTe_2$ (c), respectively.

To provide a more quantitative and experimentally grounded evaluation, we have additionally estimated the carrier density from the Fermi surface (FS) area extracted from the ARPES data, following the Luttinger theorem as suggested. As shown in the ARPES FS map of Rb/ML $IrTe_2$ (Fig. **S**4), the FS consists of a single electron pocket centered at the Γ point. The carrier concentration is extracted from the Fermi surface via Luttinger's theorem

$$n = \frac{1}{(2\pi)^3}\int dk\, \theta(\mu_0 - \epsilon_k)$$

, where θ is step function, μ_0 is unperturbed chemical potential.

The extracted carrier density from Luttinger theorem is then ~$2.6 \times 10^{14}\ cm^{-2}$. The corresponding carrier concentration is then 0.35 electron per unit cell. This value is significantly larger than the doping level which used in DFT calculation (~0.05 electrons).

Despite this quantitative difference, our DFT results demonstrate that even a relatively small electron doping of ~0.05 electrons per unit cell is sufficient to strongly suppress the instability at the M point. This is evidenced by the reduction of the peak in the calculated electronic susceptibility (Figs. 4d and **S**5) and the disappearance of the corresponding phonon softening (Fig. 4e). These results indicate that the instability of the 2 × 1 dimerized phase is highly sensitive to carrier doping, and that the qualitative trend is already captured at low doping levels.

Furthermore, the experimentally observed FS topology is qualitatively different from that expected for a pristine undistorted 1 × 1 structure. As shown in the ARPES data (Fig. **S**4a), the FS does not match the calculated FS of the 1 × 1 phase (Figs. **S**4b,c), but instead exhibits features consistent with a reconstructed electronic structure. This suggests that the suppression of the 2 × 1 dimerized phase does not lead to a simple recovery of the pristine 1*T* structure. Rather, the system evolves toward a BL-like electronic configuration, which is known to host charge-ordered phases with longer periodicities (e.g., 3 × 1 or 5 × 1), consistent with our ARPES observations.

Taken together, these results indicate that (i) the experimentally estimated carrier density reflects a reconstructed metallic state beyond a simple rigid-band doping picture, and (ii) the collapse of the dimerized phase is driven by carrier-induced modifications of both the Fermi surface topology and the associated electronic instability, rather than a direct transition to a pristine 1*T* phase.

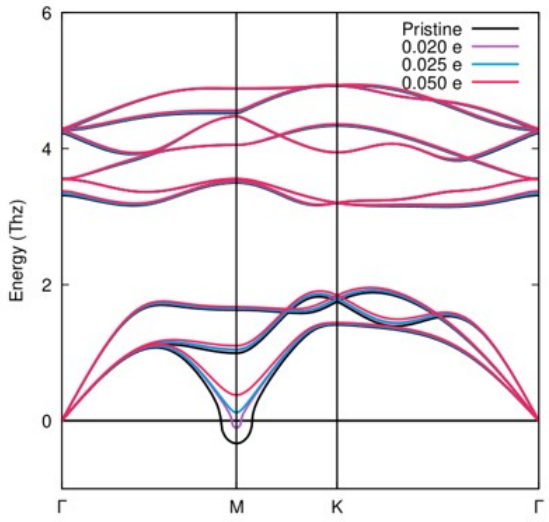

Figure S5. Electron doping dependent phonon dispersion of ML $IrTe_2$. Calculated phonon dispersion relations along the high-symmetry directions (Γ–M–K–Γ) for pristine and electron-doped ML $IrTe_2$. The results are shown for pristine (black), 0.020 *e* (purple), 0.025 *e* (blue), and 0.050 (red) *e* doping levels per unit cell.